Aberrant ZNF423 impedes B cell differentiation and is linked to adverse outcome of *ETV6-RUNX1* negative B precursor acute lymphoblastic leukemia

Lena Harder,[1] Georg Eschenburg,[1] Antonia Zech,[1] Neele Kriebitzsch,[1,7] Benjamin Otto,[2,3] Thomas Streichert,[2] Anna-Sophie Behlich,[1] Kevin Dierck,[1] Bine Klingler,[1] Arne Hansen,[4] Martin Stanulla,[5] Martin Zimmermann,[5] Elisabeth Kremmer,[6] Carol Stocking,[7] and Martin A. Horstmann[1]

[1]Research Institute Children's Cancer Center and Clinic of Pediatric Hematology and Oncology, University Medical Center Hamburg-Eppendorf, 20246 Hamburg, Germany
[2]Institute of Clinical Chemistry, University Medical Center Hamburg-Eppendorf, 20246 Hamburg, Germany
[3]Department of Internal Medicine, University Medical Center Hamburg-Eppendorf, 20246 Hamburg, Germany
[4]Department of Experimental Pharmacology and Toxicology, University Medical Center Hamburg-Eppendorf, 20246 Hamburg, Germany
[5]Department of Pediatric Hematology and Oncology, Hannover Medical School, 30625 Hannover, Germany
[6]Institute of Molecular Immunology, Helmholtz Center Munich, 81377 Munich, Germany
[7]Heinrich-Pette-Institute, Leibniz-Institute for Experimental Virology, 20251 Hamburg, Germany

Differentiation arrest is a hallmark of acute leukemia. Genomic alterations in B cell differentiation factors such as PAX5, IKZF1, and EBF-1 have been identified in more than half of all cases of childhood B precursor acute lymphoblastic leukemia (ALL). Here, we describe a perturbed epigenetic and transcriptional regulation of *ZNF423* in ALL as a novel mechanism interfering with B cell differentiation. Hypomethylation of *ZNF423* regulatory sequences and BMP2 signaling result in transactivation of *ZNF423*α and a novel *ZNF423*β-isoform encoding a nucleosome remodeling and histone deacetylase complex–interacting domain. Aberrant ZNF423 inhibits the transactivation of EBF-1 target genes and leads to B cell maturation arrest in vivo. Importantly, *ZNF423* expression is associated with poor outcome of *ETV6-RUNX1*–negative B precursor ALL patients. Our work demonstrates that ALL is more than a genetic disease and that epigenetics may uncover novel mechanisms of disease with prognostic implications.

CORRESPONDENCE
Martin A. Horstmann:
horstman@uke.de

Abbreviations used: 5A2D, 5′-aza-2-deoxycytidine; ALL, acute lymphoblastic leukemia; CBMC, cord blood MNC; CGI, CpG island; HSC, hematopoietic stem cell; HSCT, HSC transplantation; MNC, mononuclear cell; NID, NuRD-interacting domain; NSG, *NOD.Cg-Prkdc*^{scid} *Il2rg*^{tm1Wjl}*/SzJ*; NuRD, nucleosome remodeling and histone deacetylase complex.

The acute lymphoblastic leukemia (ALL) is the most common malignancy of childhood. The underlying disease mechanisms leading to overt leukemia are still incompletely understood, including the maturation arrest as a hallmark of the leukemic phenotype. Various structural and numerical chromosomal aberrations have been identified, some of which are being used in risk stratification, such as *ETV6-RUNX1* or *BCR-ABL1* rearrangements of the mixed-lineage leukemia (MLL) gene, hypodiploidy, and hyperdiploidy (Pui et al., 2004; Mullighan et al., 2009). These chromosomal aberrations are considered to be the primary event in disease development, followed by a broad range of secondary mutational events. Among those aberrations, deficiencies in transcriptional regulators of B lymphopoiesis (PAX5, EBF-1, and IKZF1) have been identified that cause a differentiation arrest in lymphopoietic progenitors (Pui et al., 2004; Mullighan et al., 2007, 2009; Zhang et al., 2011). The most frequently affected factor in lymphoid development is PAX5, which is involved in 32% of B cell precursor ALL, but whose mutation status is not linked to disease outcome (Mullighan et al., 2007). Genetic alterations of *IKZF1* are less frequent, but correlate with poor outcome and

The Rockefeller University Press $30.00
J. Exp. Med. 2013 Vol. 210 No. 11 2289-2304
www.jem.org/cgi/doi/10.1084/jem.20130497

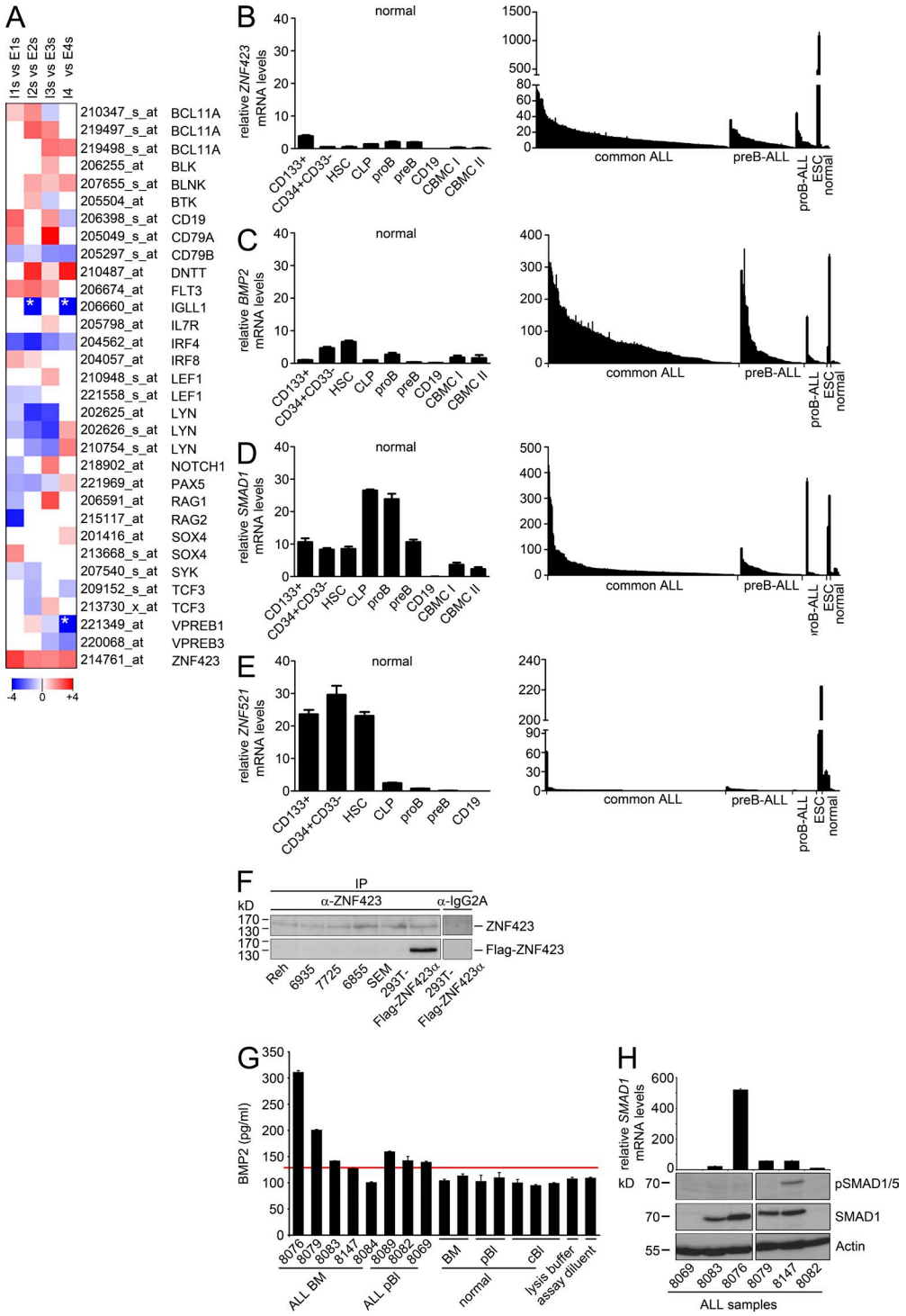

Figure 1. The BMP2–SMAD–ZNF423 axis in ALL. (A) Intraindividual transcriptome analysis. Heatmap of differentially expressed B lymphoid development–related genes in B precursor ALL versus individually matched normal B progenitor cells (n = 4 matched pairs). ID was given for each gene representative probe set. ZNF423 probe hybridizes to the 3′UTR of the gene. Color code represents Signal Log Ratio (SLR) with ceiling at max −4/+4; * indicates ceiled values. I1s-I3s, initial FACS-sorted leukemia sample; E1-4s, FACS-sorted B progenitor cells at the end of reinduction in complete remission; I4, unsorted initial leukemia sample (>90% blasts). (B–E) qPCR-based quantification of *ZNF423* (B), *BMP2* (C), *SMAD1* (D), and *ZNF521* (E) mRNA levels at various stages of hematopoietic development (left) and in primary B cell ALL (n = 200), ESC lines (H1, HES2), and normal hematopoietic cells (right). Values were normalized to β-*2-microglobulin*, *B2M* ($2^{-\Delta Ct}$*1000). Error bars represent standard deviation (SD) of technical triplicates. Cutoff is defined as double SD of highest value in the normal compartment. (F) Expression of endogenous ZNF423 protein in primary ALL and ALL cell lines. As a control, 293T cells were transfected with Flag-ZNF423α. ZNF423 was immunoprecipitated (IP) using the ZNF423 monoclonal antibody, IgG2A was used as

are associated with an increased expression of hematopoietic stem cell (HSC) genes and reduced expression of B lymphopoietic genes. Early B cell factor 1 (EBF-1), which controls essential components of the pre–B cell receptor (preBCR), is a target for monoallelic deletion in 4% of B precursor ALL (Mullighan et al., 2007, 2009). Disruption of the preBCR leads to a maturation arrest at the pre–B cell stage (Kitamura et al., 1992; Mundt et al., 2001). Overall, genome-wide analyses have identified genetic alterations of transcriptional regulators of lymphoid development in ∼60% of B-ALL patients (Mullighan et al., 2007, 2009). The cause of the differentiation arrest in the remaining cases of B precursor ALL have not been ascribed to defined genetic aberrations in transcriptional regulators of B lymphopoiesis. This suggests additional trans-regulatory and/or epigenetic mechanisms that may interfere with the B lymphopoietic transcriptional program.

Transcriptional activity is critically regulated by DNA methylation and histone modifications acting in concert to regulate gene expression (Vaissière et al., 2008). Cancer cells show global DNA hypomethylation with concomitant abnormal methylation of cytosines preceding guanosine residues in so-called CpG islands (CGIs) in gene regulatory regions (Feinberg and Tycko, 2004). DNA methylome studies of childhood ALL revealed that genetic subtypes are associated with distinct methylome profiles and that regulatory regions of B cell differentiation genes are prone to aberrant methylation (Davidsson et al., 2009). Transcriptional and epigenetic deregulation is also conferred by oncogenic fusion proteins such as ETV6-RUNX1 in ALL, which recruit co-repressor complexes containing histone deacetylases (HDAC; Zelent et al., 2004).

Murine Zfp423 is a multifunctional Krüppel-like C2H2 zinc finger factor that plays an essential role in cerebellar development, olfactory neurogenesis, and midline patterning of the central nervous system (Tsai and Reed, 1997; Hata et al., 2000; Warming et al., 2004; Cheng et al., 2007). It has been implicated as a binding partner and potent inhibitor of EBF-1 (Olf-1) that not only critically determines B cell lymphopoiesis but also olfactory neurogenesis. However, Zfp423 has not been observed in normal hematopoietic cells (Tsai and Reed, 1997, 1998). Its human homologue ZNF423 directs bone morphogenetic protein (BMP)–dependent signaling activity in a ternary SMAD1–SMAD4 transcription factor complex, whose transactivation is partially inhibited by EBF-1 overexpression, likely due to ZNF423-EBF-1 heterodimerization (Hata et al., 2000). Although there is in vitro data on the functional interaction between ZNF423 and EBF-1, there is no formal proof of its relevance to lymphopoiesis in vivo, and even less of its relevance to the pathobiology of ALL.

Here, we identify *ZNF423* as a target for epigenetic deregulation and BMP2-dependent pathways in ALL of childhood. Aberrant ZNF423 inhibits EBF-1 target genes, leads to a B cell maturation arrest in vivo and is associated with poor outcome of *ETV6-RUNX1*–negative ALL.

RESULTS

Aberrant expression of the transcriptional modulator ZNF423 in ALL

Transcriptional deregulation of essential B cell differentiation factors or their targets may critically contribute to the differentiation arrest in ALL. To address this question, comparative intraindividual transcriptome profiling of FACS-sorted leukemic versus immunologically matched normal lymphoblasts isolated from the same individual in complete remission was used to identify differentially regulated genes (Fig. 1 A). Here, we focused on a set of genes that are involved in the process of B cell differentiation (Mullighan et al., 2007). Given the genetic heterogeneity of progenitor B-ALL, a variable expression of most of the B cell differentiation–related genes was observed as anticipated, apart from a uniform down-regulation of *IRF4* and *CD79b* on the one hand and an up-regulation of *ZNF423* on the other. ZNF423 is not constitutively expressed during lymphopoiesis but is able to sequester the EBF-1 (Olf-1) transcription factor with previously described implications for olfactory neuronal differentiation (Tsai and Reed, 1997). We reasoned that a transcriptional modulator that is capable of binding EBF-1 might contribute to the B cell differentiation block, and thus we set out to define the underlying mechanism of its aberrant expression in leukemic lymphoblasts. Because ZNF423 has been described as a binding partner of the SMAD1–SMAD4 complex, we first addressed the activity of BMP-dependent signaling pathways in ALL. The expression of *BMP2*, *SMAD1*, and *ZNF423* was assessed at the transcriptional level in primary B precursor ALL samples (n = 200) using quantitative real-time PCR (qPCR; Table S1). The majority of leukemic samples exhibited a substantially increased expression of *BMP2* and *ZNF423* transcripts in comparison with normal cells purified by FACS sorting from the healthy lymphopoietic compartment at various stages of differentiation (Fig. 1, B and C). Increased expression of *SMAD1* occurred less frequently (Fig. 1 D). *ZNF423* and *SMAD1* transcripts showed a moderate correlation (r = 0.32793; $P < 10^{-4}$). However, both factors revealed a strong association with *ETV6-RUNX1*–rearranged ALLs (Table 1 and Table 2). Aberrant expression of *ZNF423* was maintained in relapsed ALL of initially positive samples (unpublished data). Interestingly, human embryonic stem cell lines H1 and HES2 revealed similarly high *BMP2* and *SMAD1* transcript levels as primary ALL cells and an extraordinarily high expression of *ZNF423* supporting its functional role in early human development. In contrast, the ZNF423 homologue ZNF521 (Evi3,

isotype control. Protein precipitates were immunoblotted for ZNF423 and FLAG-tag. (G) ELISA-based detection of soluble BMP2 in BM, peripheral blood (pBl), and cord blood (cBl) plasma from ALL patients and healthy donors. Lysis buffer and assay diluent display the negative controls. Red horizontal line, threshold value of maximum expression in normal cells. Error bars represent SD of technical triplicates. (H) Immunoblot analysis of SMAD1 and phosphoSMAD1/5 protein expression in primary ALL samples including corresponding *SMAD1* transcript levels (refer to D). Actin was used as loading control.

Table 1. Relationship between expression of *ZNF423*, *BMP2*, and *SMAD1* in B-ALL

	ZNF423	*BMP2*	*SMAD1*
ZNF423	1.00000	0.10372; P = 0.1544	0.32793; P < 0.0001
BMP2	0.10372; P = 0.1544	1.00000	0.24840; P = 0.0005
SMAD1	0.32793; P < 0.0001	0.24840; P = 0.0005	1.00000

Spearman correlation between *ZNF423*, *BMP2*, and *SMAD1* expression in $n = 190$ B-ALL.

EHZF) that has been implicated in hematopoiesis and myeloid malignancies (Bond et al., 2004) was aberrantly expressed in only 1 out of 115 tested ALL samples (Fig. 1 E). *ZNF521* exhibited a strong expression in $CD133^+$ fetal liver, as well as in umbilical cord blood stem and progenitor cells followed by a rapid decline during B cell differentiation.

Next, we addressed the components of the BMP2-dependent pathway at the protein level. Using immunoprecipitation, endogenous ZNF423 protein was detected in primary ALLs and ALL cell lines that expressed ZNF423 transcripts (Fig. 1 F). Increased plasma concentrations of secreted soluble BMP2 were detected in the BM or peripheral blood of ALL patients as determined by enzyme-linked immunosorbent-assay (ELISA; Fig. 1 G). At the basal signaling state BMP2-dependent phosphorylation of SMAD1/SMAD5 was detected in one of four tested SMAD1-expressing primary ALL samples that revealed increased concentrations of plasma BMP2. This ALL lacked a constitutively active mutation of SMAD1 and might indicate active BMP2 signaling in vivo. The usually transient nature of BMP-dependent phosphorylation upon sample processing could account for the nondetectable SMAD1/SMAD5 phosphoactivity in the remaining ALL samples (Fig. 1 H and not depicted).

Genomic profiling of *ZNF423* and B cell differentiation factors in ALL

To evaluate the mechanistic basis of aberrant *ZNF423* activation, we screened the genomic locus of *ZNF423* in 20 individually matched pairs of primary ALL with detectable *ZNF423* transcripts and corresponding normal mononuclear cells (MNCs) extracted from BM samples using high-resolution SNP array profiling. This approach revealed two cases of copy number variation at the *ZNF423* locus in ALL samples (Fig. 2 A). A hyperdiploid *ZNF423*-positive B precursor ALL with trisomy 5, 11, and 16 is associated with genomic gains, including the *ZNF423* locus on chromosome 16 and multiple loci of B cell differentiation–associated genes, including *CSF1R*, *EBF-1*, *IL7R*, *RAG1*, and *CD19*. In contrast, a near diploid ALL revealed a loss of one *ZNF423* gene copy, which nevertheless showed an elevated level of *ZNF423* transcripts, suggesting a perturbed transcriptional regulation as the underlying cause of the aberrant expression. Loss of heterozygosity of known regulators of B cell differentiation or their target genes were identified in 10 out of 20 cases, as shown in Fig. 2 A. In accordance with previous works, *PAX5* was identified as the most frequently affected gene among B cell differentiation factors followed by Ikaros (*IKZF1*) and EBF-1 (Mullighan et al., 2007). Aberrant *ZNF423* expression and copy number variations of defined B cell differentiation factors occurred neither in a mutually exclusive nor strictly coincident manner, indicating independent molecular events.

ZNF423 is a transcriptional target of BMP2 signaling in ALL

Because of the mostly intact genomic structure at the *ZNF423* locus, we set out to search for potential transregulatory mechanisms as a cause for aberrant expression of *ZNF423* in ALL. *MLL/AF4*–rearranged SEM cells were chosen from a panel of ALL cell lines as a cellular model to test the hypothesis that ZNF423 not only acts as a binding partner and transcriptional modulator of the phosphorylated SMAD1–SMAD4 complex but is also transcriptionally regulated along BMP2-induced pathways. BMP2 treatment caused a marked increase in phosphorylation of SMAD1/SMAD5 and an up-regulation of ZNF423 transcripts reaching a maximum induction after 5 h, which is similar to the direct BMP2 target gene *RUNX2* (Lee et al., 2000; Fig. 2, B and C). The transcriptional induction of *ZNF423* (as well as *RUNX2*) was also demonstrated for the BMP2 homologue BMP4, whereas BMP7, as a family

Table 2. Expression of *ZNF423*, *BMP2*, and *SMAD1* transcripts in dependence on *ETV6-RUNX1* status

		ETV6-RUNX1 negative	*ETV6-RUNX1* positive	All	P-value
	n	118	49	167	
ZNF423	Mean	9.25	21.28	12.78	0.0000
	Median	0.0–36.2	0.1–72.5	0.0–72.5	
	SD	7.714	18.040	12.893	
BMP2	Mean	53.42	70.38	58.40	0.0017
	Median	0.1–299.2	3.0–272.6	0.1–299.2	
	SD	68.197	57.352	65.491	
SMAD1	Mean	11.71	56.82	24.95	0.0000
	Median	0.0–82.0	0.6–402.3	.0.–402.3	
	SD	12.881	75.978	47.015	

Distribution analysis of *ZNF423*, *BMP2*, and *SMAD1* in *ETV6-RUNX1*-positive or -negative samples by *U* test. SD, standard deviation; p, P value.

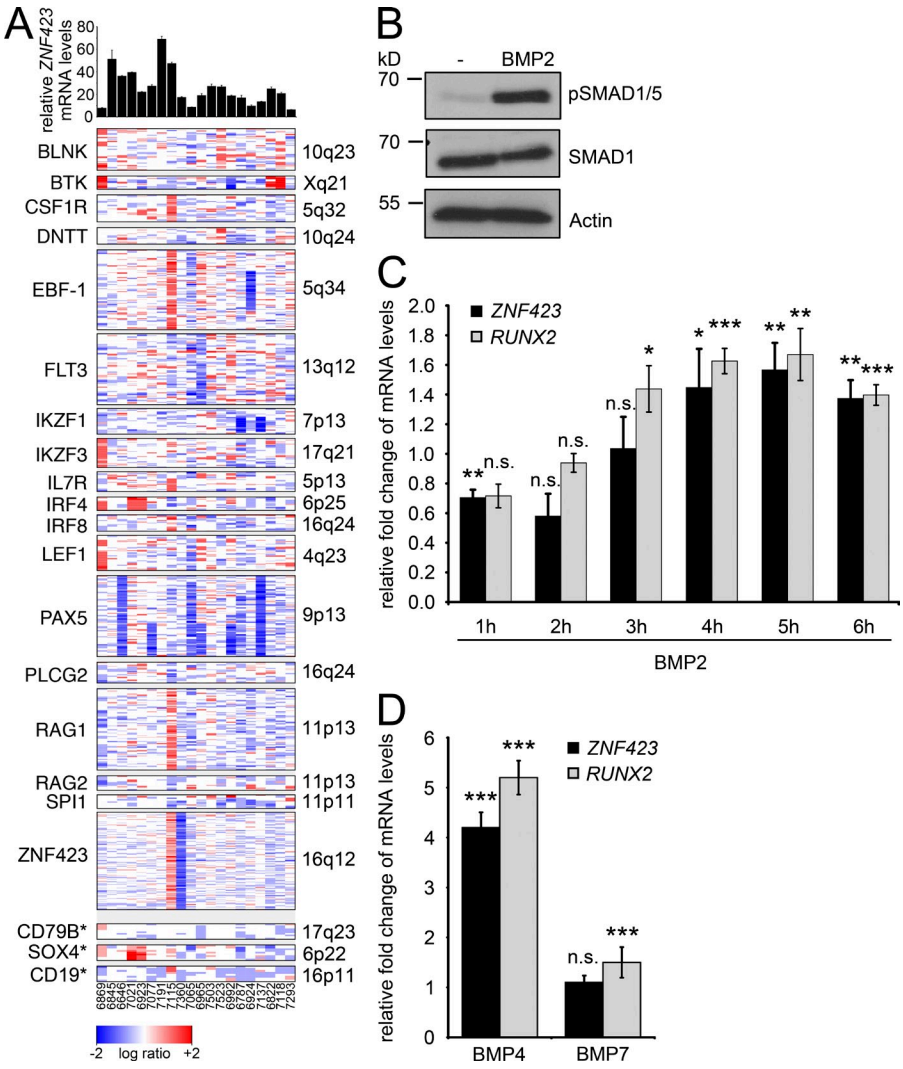

Figure 2. *ZNF423* is transcriptionally up-regulated upon BMP signaling. (A) High resolution genomic profiling of *ZNF423* and B cell differentiation related factors in ZNF423$^+$ ALL. For indicated *ZNF423* expression refer to Fig.1 B. Values were normalized to β-*2-microglobulin*, *B2M* ($2^{-\Delta Ct}$*1000). Error bars represent SD of technical triplicates. SNP array analysis of $n = 20$ initial B-ALL samples and $n = 20$ matched MNCs from remission BM samples. Smoothed copy-number SLR exhibiting gains or losses in at least one sample were chosen. For genes marked by *, probes located in a window of ±5 kb up- and downstream of the genomic locus are included due to scarce coverage of SNPs in coding regions. (B) Western blot of SMAD1 and phosphoSMAD1/5. BMP2-dependent SMAD1/5 phosphorylation in SEM cells treated with 100 ng/ml BMP2 1 h before lysis versus solvent treated cells as control. Actin was used as loading control. Blot is representative of two experiments. (C and D) RT-PCR analysis of ZNF423 and RUNX2 after stimulation with BMP family members. SEM cells were treated with 100 ng/ml BMP2 for indicated hours (C) or for 6 h with 100 ng/ml of BMP4 and BMP7 (D). Relative fold induction was measured by qPCR ($2^{-\Delta\Delta Ct}$), normalized to *B2M* and solvent control. *RUNX2* expression was used as a positive control. Error bars represent SD of technical triplicates. Significance is calculated using $2^{-\Delta Ct}$ values by Student's *t* test (*, $P \leq 0.05$; **, $P \leq 0.01$; ***, $P \leq 0.001$; n.s., not significant). Data were reproduced in three independent experiments.

member of a distinct BMP subgroup, did not lead to a clear up-regulation of either factor (Fig. 2 D).

A novel ZNF423 isoform carrying a nucleosome remodeling and histone deacetylase complex (NuRD)–interacting domain (NID) is expressed in ALL

Based on expressed sequence tags, a ZNF423β isoform has been postulated that carries a NID at the N terminus (SRRKQAKPRSVK), corresponding to the murine Zfp423 (Gronemeyer and Zelent, 2009; Lin et al., 2004; Lauberth and Rauchman, 2006). Using 5′-RACE and an isoform-specific PCR, we detected the novel β-isoform in ALL cells (Fig. 3, A, B, and D). It is likely transcribed from a distinct β-promoter that exhibits features of a CGI, whereas *ZNF423*α is regulated by a proximally situated α-promoter, as illustrated in Fig. 3 A. The relative quantification of *ZNF423*α (NM_015069) and *ZNF423*β transcripts by qPCR revealed abundant expression of both isoforms in childhood ALL compared with normal lymphopoietic progenitor and HSCs (Fig. 3, C and D). ZNF423β may exert a stronger repressive function in transcriptional regulation compared with the α-isoform by recruitment of NuRD complexes. In embryonic stem cells, *ZNF423*β was by far the most predominant isoform.

ZNF423 expression is regulated by DNA methylation

The upstream regulatory region at the *ZNF423* gene locus contains three CGIs, two of which are localized upstream of the first exon of the β-isoform. A third one takes a central position in between both *ZNF423* promoters (CGI in Fig. 3 A). We reasoned that the central CGI might act as an enhancer on potentially both *ZNF423* isoforms. Its functional relevance is corroborated by a high degree of conservation between various mammalian species (>80% homology), as demonstrated by sequence alignment (unpublished data). To assess the transactivation potential of the central CGI, we cloned 2 kb of the *ZNF423*α- and β-promoters alone and in conjunction with the central CGI into the CpG-free luciferase vector system pCpGl (Klug and Rehli, 2006). The basal activity of both promoters was significantly enhanced when combined with the central CGI (Fig. 4 A).

Next, we assessed the methylation status of the central CGI at the *ZNF423* gene locus by bisulfite sequencing in

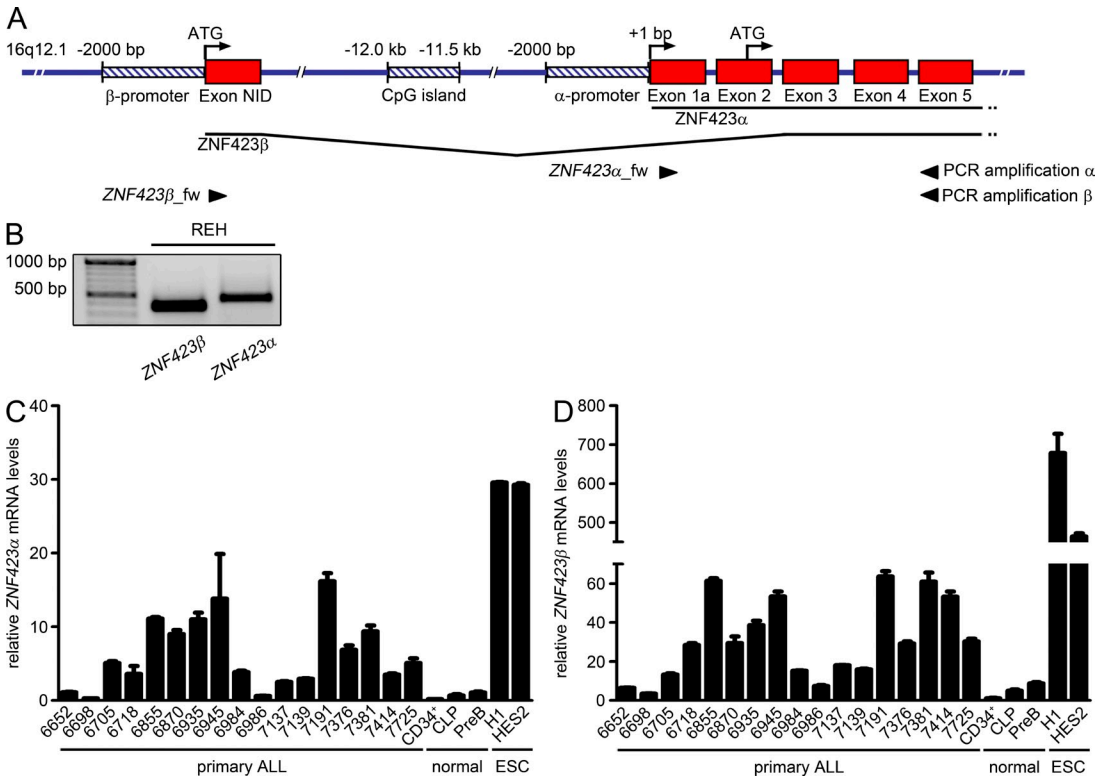

Figure 3. Identification of a novel ZNF423 isoform carrying a NID in ALL. (A) Structure of the *ZNF423* locus. Red boxes, exons; striped blue boxes, regulatory region (promoter or CGI); arrows, position and orientation of primer oligonucleotides for PCR amplification of *ZNF423* isoforms. Scheme is not drawn to scale. Adapted from UCSC genome browser. (B) PCR products of isoform-specific PCR with cDNA from REH cells. PCR products were separated by agarose gel electrophoresis and visualized by ethidium bromide staining. (C and D) Relative quantification of mRNA levels by qPCR using *ZNF423* isoform-specific primers. *ZNF423*α and *ZNF423*β were normalized to *B2M* ($2^{-\Delta Ct*}1000$). Error bars represent SD of technical triplicates.

primary ALLs, and then matched normal MNCs harvested from the patients' BM in remission and normal control cells representing various stages of lymphopoiesis. Quantitative methylation was calculated according to Lewin et al. (2004). Primary ALL samples (n = 58) revealed a significantly lower degree of methylation at multiple CpG positions of the central CGI than control lymphopoietic progenitor and HSCs, representing a broad spectrum of differentiation, including fetal liver $CD133^+$ HSCs ($P \leq 0.001$). This observation indicates a nonpermissive transcriptional state of *ZNF423* during lymphopoiesis (Fig. 4 B). MNCs purified from matched BM in remission also exhibited a substantially higher degree of methylation of the central CGI than primary ALL cells. Intriguingly, in analogy to primary ALL, the embryonic stem cell lines H1 and HES2 showed a rather hypomethylated CGI corresponding to a high level of *ZNF423* transcripts (Figs. 1 B and 4 B). Hence, the hypomethylation of ZNF423 regulatory sequences in ALL reflects a dysregulated epigenetic state, which may reactivate a transcriptional program normally encountered at an immature developmental stage.

To evaluate site-specific effects of DNA methylation on transactivation of the *ZNF423* α-promoter, we introduced point mutations into differentially modified CpG dinucleotides in the central CGI (CGI positions: 102, 183, 220, and 250). The single mutation at position 250 and the combined mutation of all four indicated CGI sites reduced *ZNF423* promoter activity in the nonmethylated state. As anticipated M.SssI-dependent methylation of all CpGs in the wild-type sequence led to a nearly complete loss of transcriptional activity. Mutagenesis of individual CpG dinucleotides in the CGI rescued promoter activity under M.SssI treatment, depending on the mutation site (Fig. 4, C and D). In contrast, the combined mutation of significantly differentially methylated CpGs had a lesser effect, exhibiting a greater sensitivity toward M.SssI treatment compared with single mutants. This observation may be at least partially explained by a disruption of critical transactivating sites discernible by a reduction of basal luciferase reporter activity. Hence, the activity of ZNF423 regulatory sequences is not only dependent on the quantitative degree of methylation but also on its site-specific pattern.

In a reciprocal experimental approach, SEM cells were treated with the demethylating agent 5′-aza-2-deoxycytidine (5A2D). Using an isoform-specific qPCR, both *ZNF423* isoforms were markedly transactivated in a similar manner during the first 48 h of treatment. This effect was further augmented by BMP2 stimulation. After 72 h of 5A2D treatment, a decreased and differential transactivation of *ZNF423*α and *ZNF423*β was observed, but both isoforms maintained their BMP2 responsiveness (Fig. 4 E). As an internal positive control, we confirmed the transcriptional induction of *MAGE-1*, which

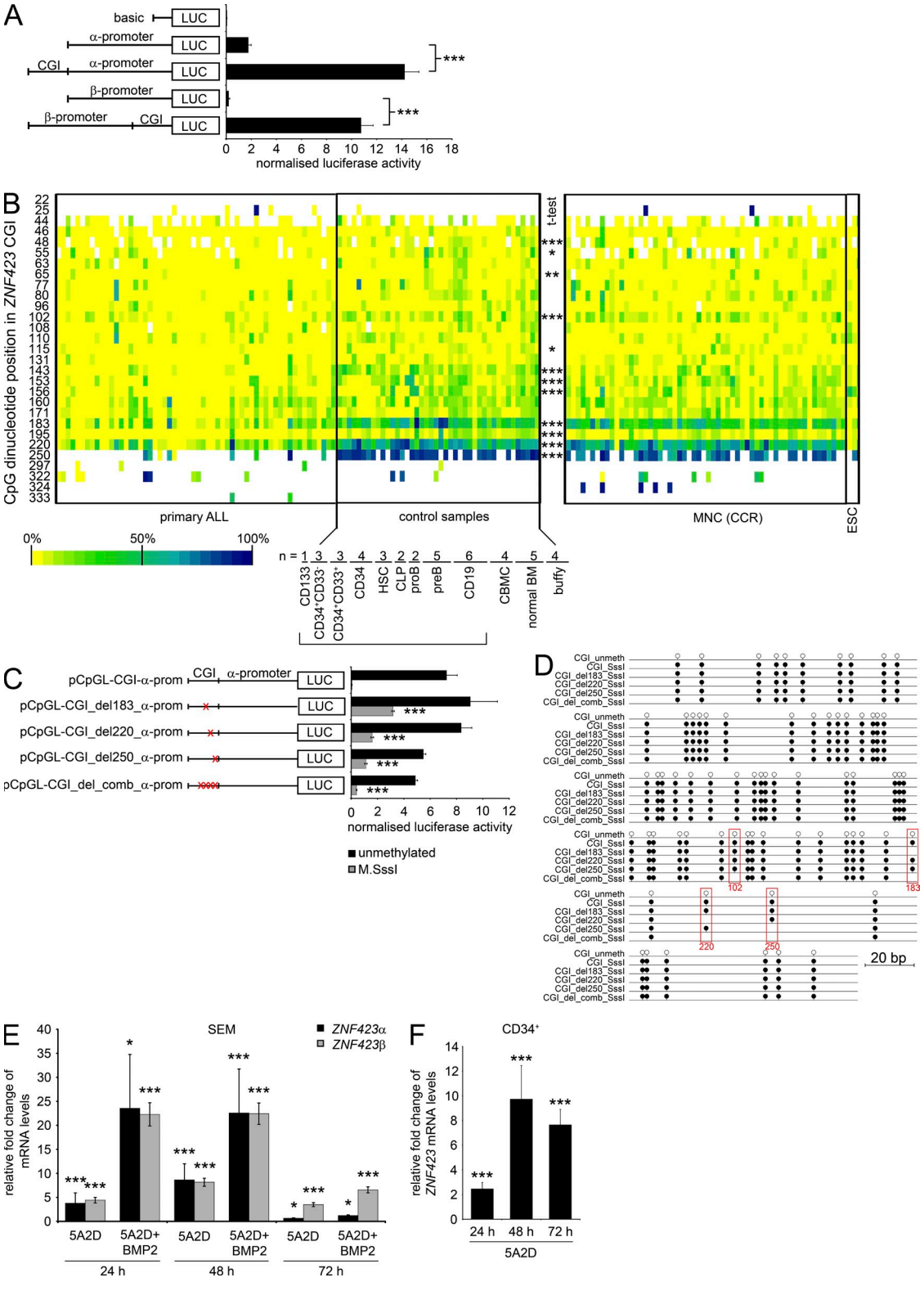

Figure 4. *ZNF423* expression is regulated by DNA methylation. (A) Transactivation of ZNF423 isoform-specific promoters in dependence of central CGI. Reporter gene assay using *ZNF423* promoters (α and β) with or without CGI after transfection in 293T cells. Firefly luciferase activity was normalized to Renilla luciferase activity. Error bars represent SD from three technical replicates. Significance is calculated by Student's *t* test, comparing indicated samples (***, $P \leq 0.001$). Data were reproduced in three independent experiments. (B) Methylation map of CpGs in the central CGI at the *ZNF423* locus. Genomic DNA from primary ALL ($n = 58$), matched BM MNCs in complete continuous remission (MNC [CCR]; $n = 58$), H1, HES2 ESC lines, and normal

was previously demonstrated to be transactivated upon 5A2D-mediated DNA demethylation (unpublished data; Ehrlich, 2002). The transcriptional up-regulation of *ZNF423* upon 5A2D treatment was recapitulated in CD34$^+$ hematopoietic stem and progenitor cells, further emphasizing the relevance of DNA demethylation to the aberrant expression of *ZNF423* in transformed lymphoblastic cells (Fig. 4 F).

ZNF423 inhibits the transactivation of EBF-1 target genes in hematopoietic cells

Previous data suggested that protein–protein interaction between ZNF423 and EBF-1 inhibits the transcriptional transactivation of EBF-1 target genes (Tsai and Reed, 1997). The physical interaction between ZNF423 and EBF1 was confirmed by co-immunoprecipitation (Fig. 5 A). To study its functional impact in a hematopoietic context, we first assessed the responsiveness of the *CD79b* promoter to either EBF-1 and/or ZNF423α by co-transfection in 293T cells. The basal *CD79b* promoter activity was significantly enhanced by wild-type EBF-1 and repressed by ZNF423α. The EBF-1–mediated increase of reporter activity was abrogated by ZNF423α co-transfection resulting in a reporter activity repressed in a concentration-dependent manner below baseline (Fig. 5, B and C). In line with previous studies, *CD79b* promoter activity was not affected by co-transfection of wild-type PAX5, and thus was excluded as a co-regulatory factor of *CD79b* (unpublished data; Nutt et al., 1998). As a next step, we performed an EBF-1 interaction domain mapping of ZNF423 by constructing various zinc finger deletion mutants to pinpoint the EBF-1–binding sites (Fig. 5 D). The last three zinc fingers have been identified as the heterodimerization domain for EBF-1 in rat Zfp423 (Tsai and Reed, 1998). Zinc fingers 2–8 represent the DNA-binding domain for ZNF423-EBF-1 heterodimers, zinc fingers 9–13 form the DNA binding domain for ZNF423-SMAD complexes, and zinc fingers 14–19 bind the phosphorylated SMAD1–SMAD4 complex (Hata et al., 2000). Surprisingly, the generation of a C-terminal deletion mutant (ZNF423α Δ28-30) lacking the predicted EBF-1 interaction domain did not revert the repression of the *CD79b* promoter (Fig. 5 B). To consequently search for additional EBF-1 interaction domains, we created a variety of stably expressed ZNF423 deletion mutants, omitting individual protein domains (Fig. 5, D and F). All mutants devoid of the C-terminal zinc fingers 20–30 lost the repressive effect on the *CD79b* promoter, indicating that the EBF-1–binding domain of human ZNF423 is not restricted to zinc fingers 28–30 but extends to a region between zinc fingers 20–27 (Fig. 5 E). Other mutants with central or N-terminal deletions but an intact C terminus exhibited a pronounced repressive effect on *CD79b* promoter activity. Intriguingly, the ZNF423β isoform with the NID exerted a stronger repressive effect on the *CD79b* promoter than the ZNF423α form.

To assess the functional relevance of EBF-1 sequestration by ZNF423 independent of NuRD recruitment in hematopoietic cells, CD34$^+$ stem or progenitor cells isolated from human cord blood were retrovirally transduced using a ZNF423α-expressing vector (MYs-ZNF423α-venus) versus empty control vector (MYs-venus-control). 5 and 8 d after transduction, *EBF-1* and its target genes *CD79a*, *CD79b*, and *IGLL1* were analyzed in vitro at the transcriptional level by qPCR. Both *CD79a* and *CD79b* transcripts were significantly reduced upon enforced expression of ZNF423α (Fig. 5 G). Under the chosen experimental conditions, *IGLL1* did not show a ZNF423α-dependent transcriptional repression in vitro.

ZNF423 perturbs the in vivo differentiation process of the B cell lineage

After demonstrating that ZNF423 inhibits the transcriptional activation of lymphopoietic EBF-1 target genes in cell-based studies, we proceeded to assess the impact of aberrant ZNF423α expression in vivo in a xenograft HSC transplantation (HSCT) model (Fig. 6 A). Using two different retroviral particles carrying a venus cassette (MYs-venus-control and MYs-ZNF423α-venus), we transduced CD34$^+$ cord blood cells and transplanted ≥10^6 cells into immunodeficient *NOD.Cg-Prkdc^{scid} Il2rg^{tm1Wjl}/SzJ* (NSG) mice intratibially without further conditioning (Shultz et al., 2005). 6 wk after transplantation, animals from the control cohorts (n = 18) and ZNF423-positive cohorts (n = 17) were sacrificed and examined for human hematopoietic engraftment. BM and spleen cells were isolated and sorted by

hematopoietic cells at various stages of differentiation (n = 42) from healthy donors were sequenced after bisulfite conversion. Each row represents one cytosine in a CG dinucleotide of the analyzed sequence. For cell lineage abbreviations, refer to Figure 1. Significance is calculated by Student's t test, comparing primary ALL to immunologically characterized control samples (in brackets; *, P ≤ 0.05; **, P ≤ 0.01; ***, P ≤ 0.001). Color code represents degree of methylation in percent. White boxes indicate no sequencing data available. (C) *ZNF423* promoter activity in dependence of CPG mutational status. Disruption of CpGs was performed by site-directed mutagenesis as indicated by red marks. Combined deletion mutant (pCpGL-CGI-del_comb_α-prom) represents deletions at CGI positions 102, 183, 220, 250. Wild-type and mutated plasmids were treated with DNA-methylase M.SssI and transfected into 293T. Firefly luciferase activity was normalized to Renilla luciferase activity. Error bars represent SD from three technical replicates. Significance is calculated by Student's t test, comparing M.SssI-treated wild-type and mutated samples (***, P ≤ 0.001). Data were reproduced in three independent experiments. (D) DNA methylation pattern of central CGI. Diagram was created with BiQ Analyzer software from Max-Planck-Institute of Informatics. Drawing is to scale. White lollipop, unmethylated; black lollipop, methylated. Marked CpGs refer to heatmap in Fig. 4 B. (E and F) Expression of ZNF423 transcripts upon DNA demethylation and BMP2 stimulation. SEM cells (E) and CD34$^+$ cord blood cells (F) were treated with 3 µM 5A2D for 24, 48, and 72 h. In SEM cells, additional BMP2 treatment was performed 6 h before lysis. Relative fold induction was measured by qPCR ($2^{-\Delta\Delta Ct}$) using a ZNF423 isoform-specific primer design in SEM cells. mRNA levels were normalized to *B2M* and solvent control. Error bars represent SD out of three technical replicates. Significance is calculated using $2^{-\Delta Ct}$ values by Student's t test (*, P ≤ 0.05; **, P ≤ 0.01; ***, P ≤ 0.001; n.s., not significant). Data were reproduced in three independent experiments.

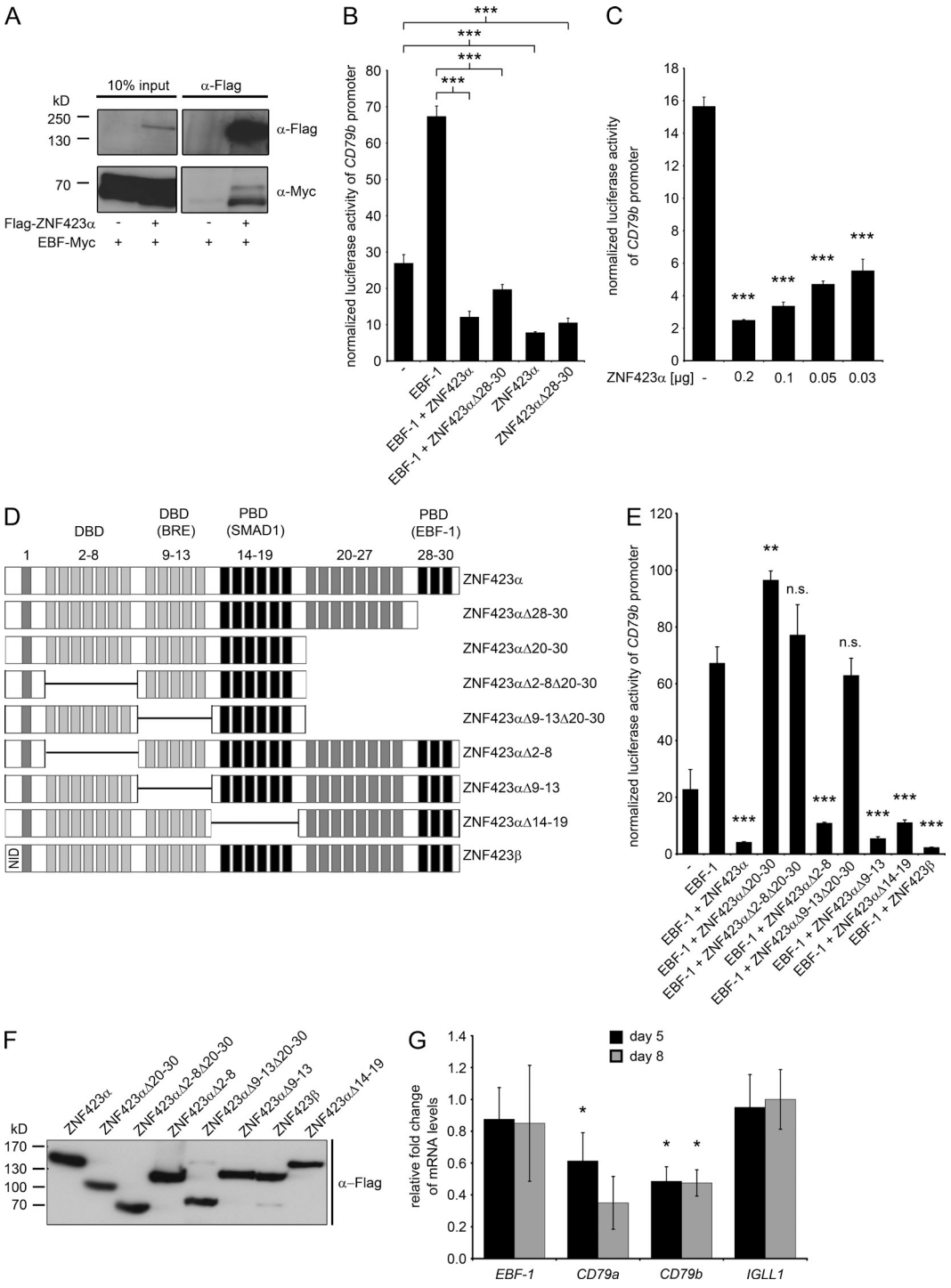

Figure 5. The interaction between ZNF423α and EBF-1 inhibits EBF-1 target gene expression in hematopoietic cells. (A) Co-immunoprecipitation of ZNF423 and EBF-1. Immunoblotting of input and eluate from Flag-IP. Detection of the transfected proteins by indicated antibodies. Binding was shown in three independent experiments. (B) Transactivation of the *CD79b* promoter upon EBF-1 and ZNF423α wild-type versus C-terminal deletion mutant ZNF423αΔ28-30. Luciferase assay was performed in 293T cells. ZNF423α plasmid was co-transfected at the indicated concentrations. Firefly luciferase activity was normalized to Renilla luciferase activity. Error bars represent SD of three technical replicates. Significance is calculated by Student's *t* test, comparing indicated samples (***, $P \leq 0.001$). Data were reproduced in three independent experiments. (C) ZNF423α concentration-dependent transactivation of the *CD79b* promoter. Luciferase assay was performed as in B. Significance of technical replicates is calculated by Student's *t* test, comparing to *CD79b* promoter baseline (***, $P \leq 0.001$). Data were reproduced in three independent experiments. (D) ZNF423 domain mapping using deletion mutants. Each box represents a C2H2 zinc finger motif. DBD, (light gray box) DNA binding; PBD (black box), protein binding; dark gray box, unknown function; black lines, deleted regions. Scheme is not to scale. (E) *CD79b* promoter activity in dependence of EBF-1 and co-transfected ZNF423 isoforms and

FACS based on reporter fluorescence. The relative quantification of EBF-1–dependent target gene transcripts revealed that the ZNF423α expression in engrafted hematopoietic cells in vivo led to a significant reduction of *CD79a*, *CD79b*, and *IGLL1* transcripts compared with empty vector control (Fig. 6 B). The comparable expression of the B cell marker CD19 in ZNF423α expressing versus nonexpressing cells indicated that ZNF423α activity perturbed lymphopoiesis after lineage commitment in our xenotransplantation model.

The stage of human B lymphopoietic differentiation can be roughly assessed by measurement of the surface markers CD34, CD19, and IgM (B cell receptor; BCR), which were used to determine the immunological phenotypes of ZNF423α-positive versus control cells after engraftment in NSG mice (Fig. 6 C). A lower frequency of cells expressing mature BCRs was observed within the ZNF423α-transduced cell population with an increased number of events for CD34 positivity, indicating a greater proportion of immature progenitor cells. Taken all cohorts together, the number of engrafted cells carrying a mature BCR was significantly reduced upon expression of ZNF423 (Fig. 6 D). In contrast, myelopoiesis as evaluated by CD33 staining in our experimental model was not affected by enforced expression of ZNF423α in $CD34^+$ stem and progenitor cells.

Expression of *ZNF423* is a prognostic factor for outcome of B precursor ALL

Given the impact of ZNF423 on B cell maturation, we investigated whether ZNF423 and its upstream regulatory pathway were associated with the event-free survival of ALL patients. Statistical analyses were performed in B precursor ALL patients ($n = 190$) enrolled in CoALL 97 and 03 trials, who underwent a uniform treatment stratified according to clinical, immunological and genetic risk features (Escherich et al., 2010). Since *ZNF423* showed a strong association with the *ETV6-RUNX1* fusion gene (Table 2), which is a dominating marker of favorable outcome, we performed Kaplan-Meier analyses on *ETV6-RUNX1*-negative ALL patients ($n = 118$). Poor prognosis *BCR-ABL*-positive ALLs and infant leukemias were excluded from the outcome analyses, since they received a different treatment (Fig. 7). Intriguingly, six of seven *BCR-ABL*–positive ALLs revealed an increased expression of *ZNF423* in contrast to only one in five *MLL*-rearranged cases (Table S1).

We defined the median of *ZNF423* and *SMAD1* expression values as the cutoff for classification of the patients into two groups for event-free survival analyses. This threshold value is two times greater than the median *ZNF423* expression value in the *ZNF423* low-expressing group. Overall, *ZNF423* low- versus high-expressing *ETV6-RUNX1* negative ALL differ on average by a factor of four. A high level of *ZNF423* expression was associated with an adverse outcome, whereas a low level of *ZNF423* expression was associated with favorable outcome (Fig. 7 A; $P = 0.015$). These findings were in line with an association of high *ZNF423* transcript levels with elevated levels of minimal residual disease measured at the end of induction treatment (d28) by qPCR ($P < 0.01$; Fisher's exact test; Table S1). In analogy to *ZNF423*, high expression of BMP2-dependent *SMAD1* was predictive of poor outcome, and low expression of *SMAD1* was predictive of good outcome in the same cohort of patients (Fig. 7 B; $P = 0.047$). As anticipated, the expression of *ZNF423* did not significantly affect outcome prediction of *ETV6-RUNX1* fusion positive B precursor ALL in a separate subgroup analysis (data not shown). Based on the median expression values of *ZNF423* and *SMAD1*, multivariate analyses of the CoALL 97 and 03 cohorts were also performed including genetic and clinically important parameters. Multivariate testing demonstrated that *ZNF423* (and also *SMAD1*) expression predicted ALL outcome independently of clinical and genetic risk features such as patient age, white blood cell count and *ETV6-RUNX1* rearrangement (Fig. 7, A and B).

DISCUSSION

Based on comparative intraindividual transcriptome analyses, we identified the abnormal up-regulation of the transcriptional modulator ZNF423 in B precursor ALL. We found that epigenetic deregulation at the genomic *ZNF423* locus leads to a permissive transcriptional state of *ZNF423*, which is activated by BMP2 signaling in ALL. Aberrant ZNF423 inhibits the transactivation of EBF-1 target genes, perturbs B cell differentiation in vitro and in vivo, and is linked to an adverse outcome of *ETV6-RUNX1*–negative ALL patients on CoALL treatment protocols.

The rat homologue Zfp423 has previously been implicated as a transcriptional partner of Olf-1/EBF-1, but formal proof of its function in lymphopoiesis has been missing (Tsai and Reed, 1997; Warming et al., 2004; Cheng and Reed, 2007). Presumptive evidence arose from studies that identified *Zfp423* as a target for retroviral integration in murine pre–B cell lymphomas and *ZNF423* expression in *BCR-ABL*–positive chronic myeloid leukemias (Warming et al., 2004; Miyazaki et al., 2009). Using a genomic PCR strategy, we excluded genomic disruption of *ZNF423* upstream regulatory sequences in primary

mutants. Luciferase assay was performed as in B. Significance of technical replicates is calculated by Student's *t* test, comparing to *CD79b* promoter activities in the presence of EBF-1 alone to cotransfected ZNF423 isoforms or mutants(**, $P \le 0.01$; ***, $P \le 0.001$; n.s., not significant). Data were reproduced in three independent experiments. (F) Expression of recombinant ZNF423 mutants. Immunoblotting of 293T cell lysates after transfection with Flag-ZNF423 mutants. Detection of the transfected proteins by anti-Flag antibody. (G) Expression of *EBF-1* and its target genes upon retrovirally forced expression of ZNF423α in $CD34^+$ stem/progenitor cells. $CD34^+$ were transduced via retroviral particles and cultured for indicated days. Relative fold change was measured by qPCR ($2^{-\Delta\Delta Ct}$). Transcript levels were normalized to *B2M* and pMYs-control cells. Error bars represent SD of mean fold induction from independent experiments (day 5, $n = 6$; day 8, $n = 4$). Significance is calculated using $2^{-\Delta Ct}$ values by Student's *t* test (*, $P \le 0.05$).

human ALL as observed in mouse models of B cell malignancies (unpublished data). Instead, we identified an epigenetic deregulation and BMP2-dependent transactivation of *ZNF423* as novel synergistic mechanisms in ALL. In a reciprocal approach, hematopoietic CD34$^+$ stem or progenitor cells that do not express *ZNF423* could be made to activate

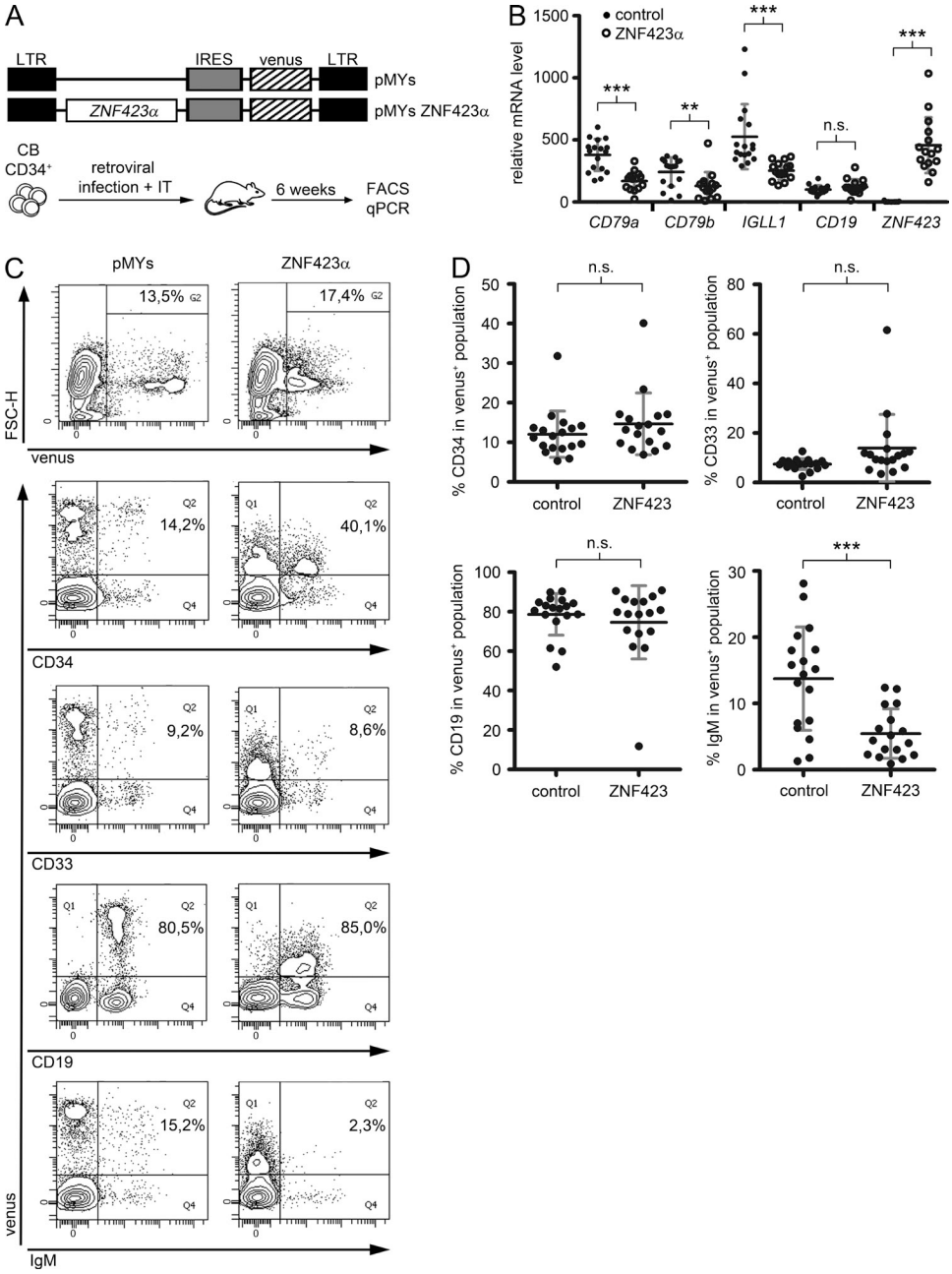

Figure 6. Forced expression of ZNF423 leads to a maturation arrest in the B cell lineage in vivo. (A) Structure of MYs retrovirus driven by long terminal repeat (LTR) sequence, venus fluorescence reporter controlled by internal ribosomal entry site (IRES). Scheme of in vivo experiments. CB CD34$^+$, cord blood CD34$^+$ stem/progenitor cells; IT, intratibial transplantation. (B) Down-regulation of EBF-1 target genes under forced ZNF423 expression in vivo. Venus positive cells from BM were FACS sorted, and mRNA was quantified by qPCR ($2^{-\Delta Ct}$*1000) for $n = 17$ control and $n = 15$ ZNF423 positive mice from $n = 3$ independent experiments. Values were normalized to *B2M*. Horizontal lines indicate mean. Error bars represent SD. Significance is calculated by Student's *t* test (**, $P \leq 0.01$; ***, $P \leq 0.001$; n.s., not significant). (C) Contour plots of FACS-based immunophenotyping of venus$^+$ BM cells from two representative animals with similar engraftment. Percentage represents positive cells in the venus$^+$ population (Q2). (D) ZNF423$^+$ cells show a significant decrease in surface IgM expression. FACS-based immunophenotyping of venus$^+$ cells in the BM of control ($n = 18$) and ZNF423 ($n = 17$) mice from $n = 3$ independent experiments. Values represent the percentage of CD34$^+$, CD33$^+$, CD19$^+$, or IgM$^+$ cells in the venus$^+$ population. Horizontal lines indicate mean. Error bars represent SD. Significance is calculated by Student's *t* test (***, $P \leq 0.001$; n.s., not significant).

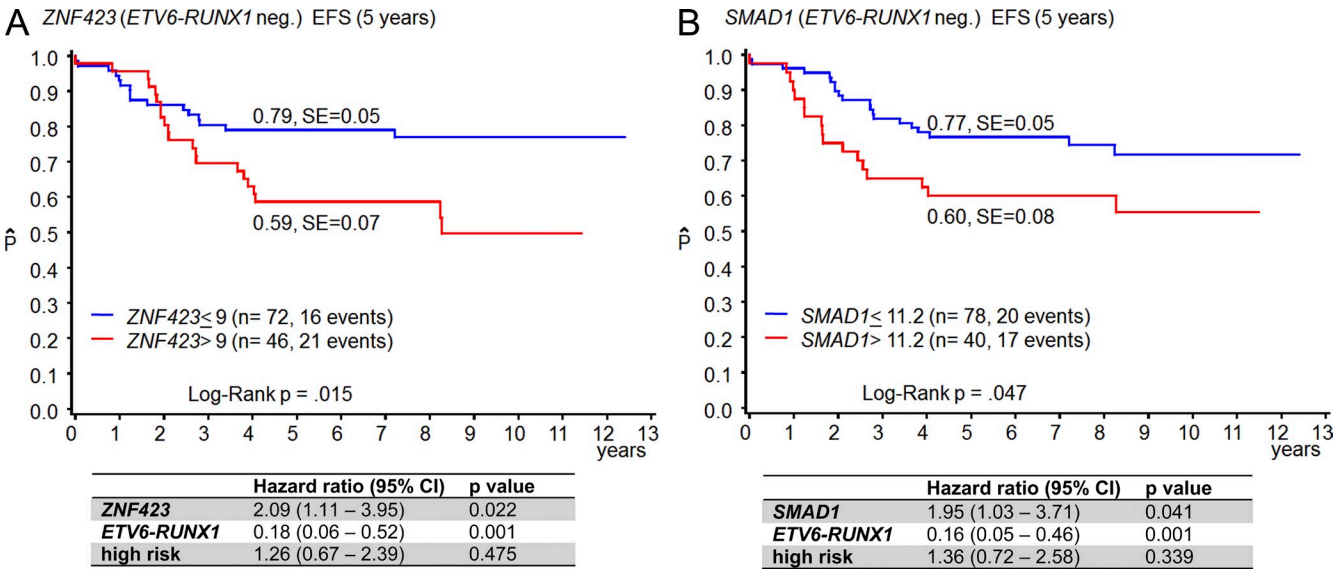

	Hazard ratio (95% CI)	p value
ZNF423	2.09 (1.11 – 3.95)	0.022
ETV6-RUNX1	0.18 (0.06 – 0.52)	0.001
high risk	1.26 (0.67 – 2.39)	0.475

	Hazard ratio (95% CI)	p value
SMAD1	1.95 (1.03 – 3.71)	0.041
ETV6-RUNX1	0.16 (0.05 – 0.46)	0.001
high risk	1.36 (0.72 – 2.58)	0.339

Figure 7. Expression of *ZNF423* and *SMAD1* is predictive for event-free survival of *ETV6-RUNX1*-negative ALL patients. (A) Kaplan-Meier analysis of the *ETV6-RUNX1*–negative CoALL 97 and 03 patient cohorts indicating an adverse outcome of patients with *ZNF423* high expressing ALL using the median of *ZNF423* as the cutoff value. The analysis was performed in $n = 118$ patients with *ETV6-RUNX1*–negative B precursor ALL. The multivariate analysis of the overall cohort including clinically relevant parameters such as *ETV6-RUNX1* rearrangement and classical high-risk features such as age and leukocyte count is presented underneath with hazard ratio and 95% confidence interval (CI). EFS, event-free survival; SE, standard error. (B) Kaplan-Meier analysis in the same cohort as in A in dependence of *SMAD1* expression revealing an adverse prognosis in ALL patients with high *SMAD1* expression using the *SMAD1* median as the cutoff value. In analogy to (A) a separate multivariate analysis identifies *SMAD1* expression as an independent risk factor in ALL.

ZNF423 by treatment with the demethylating agent 5′-aza-2-deoxycytidine.

ZNF423 appears to operate as a transcriptional modulator in independent BMP- and EBF-1–mediated reaction pathways (Hata et al., 2000). It has recently been implicated in retinoic acid–dependent differentiation of neuroblastoma by its association with the RARα/RXRα nuclear receptor complex (Huang et al., 2009). In ALL, the net outcome of ZNF423-modulated transcriptional activity likely depends on the relationship between varying levels of EBF-1 monomers and phosphorylated SMAD1–SMAD4 complexes, which might encounter a steric hindrance upon coincidental binding at their defined zinc finger–binding sites in ZNF423 or compete for common yet undefined ZNF423-binding sites.

Epigenetic deregulation and aberrant expression of *ZNF423* also occur in the presence of additional mutations in B cell differentiation factors and may aggravate the differentiation block and affect clinical prognosis in the context of not only *EBF-1* but also *PAX5* alterations. In line with this notion, a high cumulative number of genetic alterations targeting B cell lymphopoiesis have been reported to be associated with poor outcome. In particular, alterations of *IKZF1* have been linked to relapsing disease (Mullighan et al., 2009). Unexpectedly, aberrant *ZNF423* activity and high *SMAD1* expression were linked to an adverse outcome of ALL patients. In line with these findings ZNF423 has been linked to DNA damage response pathways, suggesting an association with chemotherapy resistance, which could account for the prognostic impact under current treatment protocols (Chaki et al., 2012). In contrast, *ZNF423* and *SMAD1* did not have prognostic impact in *ETV6-RUNX1*–rearranged ALL. ETV6-RUNX1 apparently supersedes the negative prognostic impact of *ZNF423* (and *SMAD1*) potentially by antagonizing wild-type RUNX1, incurring an inherent susceptibility to apoptosis upon cytotoxic chemotherapy (Niebuhr et al., 2013).

Although the exact stoichiometric and functional relationship between ZNF423 and EBF-1 during B cell leukemogenesis is undefined, the sequestration of EBF-1 by aberrant ZNF423 could constitute a decisive momentum in a preleukemic clone of hematopoietic stem or progenitor cells, which contributes to the initiation of disease by its interference with rising but still low levels of EBF-1 upon lineage commitment. BMP2 signaling is likely to extend the role of ZNF423 in transcriptional regulation via SMAD1-SMAD4 NuRD heterocomplex formation, whose molecular targets in ALL are unknown. The occurrence of the novel ZNF423β isoform in human ALL is analogous to murine Zfp423 that contains a NID with the Friend of GATA (FOG) repression motif, also found in many other transcriptional repressors (Gronemeyer and Zelent, 2009; Lin et al., 2004). It remains to be determined how ZNF423 integrates concomitant or sequential interactions with EBF-1 and phosphorylated SMAD1-SMAD4 complexes in ALL.

BMP2-dependent transactivation of ZNF423 and the formation of a ternary SMAD1–SMAD4–ZNF423 complex may physiologically operate in embryonic rather than HSCs,

as indicated here by data on HES2 and H1 cells. In olfactory neurogenesis, Zfp423 has been demonstrated to operate as a lineage switch factor that arrests olfactory receptor neurons at an immature stage, with perturbed olfactory receptor gene selection and expression (Cheng and Reed, 2007). A similar role for ZNF423 in normal B lymphoid development seems unlikely, as *ZNF423* was detectable in neither fetal HSCs nor in postnatal lymphopoietic cells, although a minor fraction of cells at an intermediary developmental stage with expression of *ZNF423* could have been missed or, alternatively, the sorting strategy applied in this study did not comprise the full complement of intermediary stages of differentiation. However, expression of *ZNF423* and subsequent inhibition of EBF-1 likely reflect abnormal molecular events that are not compatible with regular lymphopoiesis.

Collectively, our data show a causal role for ZNF423 in ALL by its interference with B cell differentiation and potentially by transcriptional modulation of SMAD1–SMAD4–dependent target genes. ZNF423 is associated with an adverse outcome of patients with ALL. Its predictive value will have to be tested in prospective trials in childhood ALL.

MATERIALS AND METHODS

Patient samples. All clinical samples were obtained with written informed consent of the patients' parents or legal guardians with approval by Institutional Ethics Boards. Patients were recruited by the COALL multicenter trial group (Germany) and enrolled in trials COALL 97 and 03. For patients' characteristics and clinical data refer to Table S1.

Mice. *NOD.Cg-Prkdc^{scid} Il2rg^{tm1Wjl}/SzJ* (NSG) mice were obtained from Charles River and were kept at the University Medical Center Hamburg-Eppendorf animal facility according to institutional animal care guidelines. Xenotransplantations of human CD34$^+$ cells were performed by intratibial injection into unconditioned 6–8-wk-old mice according to animal care regulations after approval by legal authorities (Commission on Animal Experiments, City of Hamburg, reference 55/08). Intratibial injections were performed under anesthesia (ketamine/rampen, Albrecht/Braun) at a dose of 200 mg per kg body weight. For pain relief, mice were treated with caprofen (Pfizer) at a dose of 6 mg per kg body weight for 3 d. Animals were kept under antibiotic prophylaxis (Baytril; Bayer). 6–12 wk after transplantation, mice were sacrificed. BM cells were isolated by flushing the femur and tibia with PBS. Spleen cell suspensions were prepared by tamping the spleen through a nylon mesh. MNCs of both tissues were isolated by density gradient separation. Engraftment and differentiation of human cells in the BM and spleen were analyzed using FACS.

Primary cells and cell lines. Primary CD34$^+$ cells were obtained from human cord blood samples, collected from healthy donors with approval by the Institutional Ethics Board. CD133$^+$ fetal liver cells were obtained from StemCell Technologies, Inc. RNA and genomic DNA from embryonic stem cell lines H1 and HES2 were isolated from cell culture leftover materials in accordance with national law. Cord blood MNCs (CBMCs) were separated by gradient centrifugation (Biocoll separation solution; Biochrom). Primary CD19$^+$ cells were isolated from buffy coats using CD19 MicroBeads according to manufacturer's instructions (MACS; Miltenyi Biotec). CD34$^+$ cells were isolated using the human CD34 selection kit for EasySep magnet from StemCell Technologies, Inc. following manufacturer's instructions. CD34$^+$ cells were cultured in StemSpan SFEM (StemCell Technologies, Inc.) with 2% L-glutamine, 2% penicillin/streptomycin, 100 ng/ml hFlt3-liter, 100 ng/ml hSCF, 20 ng/ml hTPO, and 20 ng/ml hIL6 (cytokines purchased from CellSystems). CD34$^+$CD33$^{+/-}$ cells were isolated by FACS sorting. REH and SEM cells were cultured in RPMI supplemented with 10% FCS and 1% L-glutamine. 293T HEK cells were cultured in DMEM supplemented with 10% FCS, 2% L-glutamine, 1% sodium pyruvate, and 2% Hepes. BMP2/4 (HumanZyme) were reconstituted in 4 mM HCl and 0.1% BSA and BMP7 (USBiological) in 20 mM acetic acid, and used at a final concentration of 100 ng/ml. Stimulation was performed for indicated times. As controls, cells were treated with solvents in analogous ways. 5-aza-2′-deoxycytidine (Sigma-Aldrich) was dissolved in water and used at a concentration of 3 µM. For transcription analysis, cells were treated for 24, 48, and 72 h, respectively. Additional BMP2 stimulation was done 6 h before lysis. Control experiments were performed using solvents. Transfection of 293T cells was performed using Lipofectamine2000 (Invitrogen) according to the manufacturer's instructions. Genomic DNA from cells was isolated with QIAamp DNA Blood Mini kit (Roche). RNA isolation was performed after TRIZOL lysis (Invitrogen) according to manufacturer's instructions.

Flow cytometry. FACS was performed using BD FACS Canto and BD FACS Aria machines. The following antibodies were used: CD38-PE-Cy7 (BD), CD34-FITC/-APC (Beckman Coulter), CD10-APC-Cy7 (Beckman Coulter), CD19-PETexasRed/-APC (Beckman Coulter), IgM-APC (BioLegend), CD33-APC (BioLegend). Umbilical cord blood CD34$^+$CD33$^+$ cells were isolated by FACS sort. HSC (CD38$^-$CD34$^+$CD10$^-$CD19$^-$), common lymphoid progenitor (CLP; CD38$^+$CD34$^+$CD10$^+$CD19$^-$), pro–B (CD38$^-$CD34$^+$CD10$^+$CD19$^+$), and pre–B (CD38$^+$CD34$^+$CD10$^+$CD19$^+$) were purified from BM of healthy patients in complete continuous remission by FACS sort.

Viral transduction. Viral particles were produced using 293T cells after transfection with the ProFection Mammalian Transfection System – Calcium Phosphate (Promega). pRMYs-iV, pMDLg-pRRE, and phCMV-RD114env plasmids were used for retrovirus production. Viral supernatants were harvested every 24 h for 3 d. Infections of CD34$^+$ cells were done using RetroNectin from Takara Bio Inc. following the manufacturer's instructions.

Reporter assays. Promoter studies were performed with the Dual-Luciferase Reporter Assay System from Promega, following the manufacturer's instructions. PCR primers for promoter cloning are listed in Table S2. The following vectors were used: pCpGL-basic, pGL3-basic, pCpGL-CMV/EF1, pGL-control, and pRL-TK (Renilla). Firefly luciferase activity was normalized to Renilla luciferase activity.

PCR and RACE. DNA amplifications for cloning were performed by PCR with Platinum Taq DNA polymerase (Invitrogen). PCR products were separated by agarose gel electrophoresis. Identification of unknown 5′ sequences was performed using 5′-3′-RACE kit (Roche) according to the manufacturer's instructions. Isoform-specific primers for *ZNF423*α and β are listed in Table S2.

Plasmids and cloning strategy. An ∼2,000-bp fragment of the *CD79b* promoter (−2,000 bp to −1 bp) was amplified by PCR (5′-CCACGGGATGTGTGTGTCTTCCCT-3′ and 5′-CCTGTCCCCTCCCCGCCTCT-3′). PCR product was cloned into pGL3-basic vector in *E. coli* JM109 competent bacteria. For studies of the *ZNF423* promoters and the *ZNF423*-CpG-island, the fragments were amplified by PCR and cloned into the CpG-free pCpGL-basic luciferase vector in *E. coli* PIRI-competent bacteria, provided by M. Klug (University Hospital Regensburg, Regensburg, Germany; Klug and Rehli, 2006). The ∼2,000-bp fragment of the *ZNF423*α-promoter (−2000 bp to +29 bp) was amplified using the primers fw 5′-GATCTCAGCGGGAGCAGGGATCAGAC-3′ and rev 5′-CATGGGGGGGACATTCCGGAGGGTTTG-3′. The ∼260-bp fragment of the CGI was amplified using the primers fw 5′-ATCTGCAGGGGAATGGCCCTGCGGCTGT-3′ and rev 5′-GTGGGATCTGAACCCTCCACGG-3′. The *ZNF423*β-promoter (−2000 bp to +40) was amplified by PCR with the primers fw 5′-CGCGGGGAGGGGGTGCT-3′ and rev 5′-CGCCTGCTTCCGCCTGGACA-3′. For ZNF423, EBF-1, and PAX5 expression, the following plasmids were used:

pcDNA3.1_Flag_hZNF423α, pcDNA3.1_Flag_hEBF-1wt, pCMV6entry-hEBF-1-Myc, and MIGR1_hPAX5wt.

Mutagenesis. Conversion of single nucleotides, as well as deletions and insertions, were performed by PCR mutagenesis with the QuickChange lightning site-directed mutagenesis kit (Agilent Technologies) according to the manufacturer's instructions. PCR primers are listed in Table S2. The truncated *ZNF423* transcripts were generated by mutation of the pcDNA3.1_Flag_hZNF423α vector. The following amino acid residues were mutated to stop: ZNF423αΔ20-30, Lys^{805} (TAG) and ZNF423 αΔ28-30, Gly^{1118} (TAA). Insertions and deletions were done between the following sites: Δ2-8, Pro^{137}/Arg^{346}; Δ9-13, Val^{408}/Lys^{589}; and Δ14-19, Glu^{631}/Ser^{804}. For ZNF423β amino acid, His^{1} to Arg^{4} were exchanged by Ser-Arg-Arg-Lys-Gln-Ala-Lys-Pro-Arg-Ser-Val-Lys (5′-TTTCACCGAGCGCGGCTTC-GCCTGCTTCCGCCTGGA-3′).

qPCR. For qPCR, TRIZOL-isolated RNA was reverse transcribed to cDNA by M-MLV reverse transcription from Promega for 1 h at 37°C using random primers (Promega). qPCR was performed with SYBR Green I (Roche), according to the manufacturer's instructions. Relative mRNA levels were depicted after normalization to β-*2-microglobulin* (*B2M*; $2^{-\Delta Ct}$*1000) as a reference gene. Primer sequences are listed in Table S2. To display relative fold changes, unknown samples were normalized to controls ($2^{-\Delta\Delta Ct}$). Significance was calculated using the $2^{-\Delta Ct}$ values by Student's *t* test.

Gene expression array. For a comparative matched pair expression analysis, single primary leukemia cells and normal lymphoblasts were isolated from the same individual, using a MoFlow Cytomation instrument by CD34, CD10, and CD19 staining. Total RNA was isolated from a minimum of 4×10^3 MNCs. Quality and concentration of isolated RNA was determined using the Agilent RNA 6000 Nano kit on an Agilent Bioanalyzer. Total RNA underwent linear amplification in a two-step procedure and was labeled and hybridized to each array according to the manufacturer's instructions using the small sample protocol. Human GeneChip U133A arrays (Affymetrix) were then washed using Affymetrix Fluidics Station 400 and scanned using a HP GeneArray scanner. The array image was acquired using the Affymetrix GeneChip Microarray Suite 5.0. Software. The samples were normalized using the MAS5 method and scaled to a target value of 100. Expression data are accessible at the Gene Expression Omnibus under accession no. GSE42221.

Microarray analysis. The expression data of four different human initial leukemias (I1s, I2s, I3s, I4; s, sorted cellular material) were independently filtered based on defined cutoff criteria such as present call; signal intensity (SI) ≥20; increase (I) or decrease call (D); change p-value ≤0.003 for I / ≥0.997 for D and signal log ratio (SLR) ≥0.5849 for I / ≤−0.415 for D (equivalent to 1.5x up- or down-regulation), which arose from the comparison with the corresponding remission material (E1s, E2s, E3s, and E4s) as control. All four comparisons were initially scaled to a target signal of 100. All genes that met these cutoff criteria were therefore considered to be differentially expressed, as depicted in the heatmap.

High-resolution genomic profiling. Genomic DNA was isolated from initial ALL samples and matched MNC from remission BM using the QIAGEN DNA Blood Mini kit following the manufacturer's instructions. Sample preparation, hybridization, and staining were performed according to the manufacturer's standard protocol for Affymetrix GenomeWide Human SNP 6.0 microarrays. Arrays were scanned on an Affymetrix 3000 7G GeneChip scanner using the Affymetrix Command Console Software. Processing of the raw signals and raw copy-number calculation were performed using the CRMA (version 2) procedure (aroma.affymetrix package version 2.0.0) for R statistical platform (version 2.12.1) according to the aroma.affymetrix vignette for paired total copy-number analysis. CBS algorithm (DNAcopy package version 1.24.0) was then applied to perform segmentation. Expression data are accessible at the Gene Expression Omnibus under accession no. GSE42056.

ZNF423 monoclonal antibody. The rat monoclonal ZNF423 antibody was generated in Lou/c rats. N-terminal epitope amplification was done by PCR with Platinum Taq DNA polymerase (Invitrogen) and following primers: 5′-GTTCGCAAGCTGCACAAGAAC-3′ and 5′-CACATAGTGGGTC-GACGTGGT-3′. PCR product was cloned into pGEX-2T (GE Healthcare) in *E. coli* JM109 competent bacteria. Isolation of fusion protein (size: 52 kD) was performed via glutathione Sepharose 4B (GE Healthcare) over PD-10 desalting columns (GE Healthcare). 50 µg of the purified GST-fusion protein were injected i.p. and s.c. into Lou/c rats using incomplete Freund's adjuvant supplemented with 5 nmol CpG 2006 (TIB MOLBIOL). After a 6-wk interval, a final boost with 50 µg ZNF423-GST and CpG 2006 was given i.p. and s.c. 3 d before fusion. Fusion of the myeloma cell line P3X63-Ag8.653 with the rat immune spleen cells was performed according to standard procedures. Hybridoma supernatants were tested in an immunoassay with GST-ZNF423 or an irrelevant GST-fusion protein. Antibodies from tissue culture supernatant bound to ZNF423 were detected with HRP-conjugated mAbs against the rat IgG isotypes (TIB173 IgG2a, TIB174 IgG2b, TIB170 IgG1 all from ATCC, R-2c IgG2c homemade), thus avoiding mAbs of IgM class. HRP was visualized with ready to use TMB (1-Step Ultra TMB-ELISA; Thermo Fisher Scientific). mAbs that reacted specifically with ZNF423 were further analyzed by Western blot. ZNF423 8H2 of rat IgG2a subclass was used in this study.

Co-immunoprecipitation. Protein G PLUS-Agarose (Santa Cruz Biotechnology, Inc.) was labeled with monoclonal ZNF423 or anti-Flag antibody (Sigma-Aldrich) for 3 h at 4°C. IgG2A (BD) was used as isotype control. For exogenous proteins, cells were transfected as indicated. Cells were lysed in KLB' lysis buffer (25 mM Tris, 150 mM NaCl, 5 mM EDTA, 10% glycerol, 1% Triton-X, 10 mM sodium pyrophosphate, 1 mM sodium orthovanadate, 10 mM glycerophosphate, 0.1 M PMSF, 1.5 mg/ml aprotinin, 0.5 M sodium fluoride, and 40 mM sodium pervanadate) and incubated with beads overnight. Precipitated proteins were detected by immunoblot.

Immunoblot. Cells were lysed in Tris/SDS (62.5 mM Tris pH 6.8, 2.3% SDS, 10% glycerol, 5% β-mercaptoethanol). Proteins were separated by 10% SDS-PAGE and transferred onto PVDF membranes (Immobilion-P; Millipore). Immunoblot detection was performed according to standard procedures. The following primary antibodies were used: anti-Flag (M2; Sigma-Aldrich), anti-c-Myc (9E10; Santa Cruz Biotechnology, Inc.), anti-SMAD1 (#9743; Cell Signaling Technology), and anti–phospho-SMAD1/5 (Ser463/465; 41D10; Cell Signaling Technology). HRP-coupled secondary antibodies were purchased from Dako.

BMP2 ELISA. BMP2 protein in plasma samples was detected with the BMP-2 Quantikine kit (R&D Systems) following manufacturer's instructions. KLB' lysis buffer and assay diluents were used as negative controls. Cut-off is defined as double SD of highest value in the normal samples.

In vitro DNA methylation. Plasmids were methylated in vitro using M.SssI methyltransferase (New England BioLabs) according to manufacturer's instructions. DNA methylation was confirmed by restriction with methylation-sensitive restriction enzymes HhaI and MspI (both obtained from Fermentas).

Bisulfite sequencing. Bisulfite sequencing of 166 genomic DNA samples extracted from initial ALL, individually matched MNC from BM in complete remission, embryonic stem cell lines H1, HES2, and normal B progenitor cells from various stages of B cell differentiation were performed by Epigenomics (Berlin). Significance was calculated by Student's *t* test, excluding data from unsorted MNC and embryonic stem cell lines.

Statistical analysis. Fisher's exact test and χ^2-test were used to analyze frequency tables, the Mann-Whitney *U* test was used to compare groups of patients and Spearman correlation coefficient was calculated to describe the correlation of parameters. Event-free survival was defined as the time from diagnosis to the date of last follow up in complete remission or first event. Events were resistant to therapy (nonresponse), relapse, secondary neoplasm

(SN), or death from any cause. Failure to achieve remission due to early death or nonresponse was considered as an event at time 0. The Kaplan-Meier method was used to estimate survival rates; differences were compared with the two-sided log-rank test. Cox proportional hazards model was used for univariate and multivariate analyses.

Software. Analysis of conservation of CGI between different species was performed using T-coffee-Multiple Sequence Alignment software from EMBL-EBI. Sequence information was obtained from UCSC Genome Browser. DNA methylation pattern was illustrated with the BiQ Analyzer software from the Max Planck Institute of Informatics.

Online supplemental material. Table S1 is an excel file showing Patients' clinical and pathological characteristics. Table S2 shows the sequence of oligonucleotides for qPCR and mutagenesis of CGI sequence. Online supplemental material is available at http://www.jem.org/cgi/content/full/jem.20130497/DC1.

We are grateful to J. Mühlisch for epigenetic support, H. Schweigel for help with epitope purification, B. Niebuhr for her support to establish mouse models, K. Klätschke for help with transcriptome profiling and SNP analysis, A. Düsedau for flow cytometry sorting, and J. Müller and M. Trochimiuk for help with mice experiments. Special thanks go to the midwives of the Asklepios Clinic Altona and Barmbek.

This work was supported by Fördergemeinschaft Kinderkrebs-Zentrum Hamburg, Burkhard Meyer Stiftung, Hans Brökel Stiftung für Wissenschaft und Kultur, and Madeleine Schickedanz Kinderkrebs-Stiftung.

The authors have no conflicting financial interests.

Submitted: 9 March 2013
Accepted: 22 August 2013

REFERENCES

Bond, H.M., M. Mesuraca, E. Carbone, P. Bonelli, V. Agosti, N. Amodio, G. De Rosa, M. Di Nicola, A.M. Gianni, M.A. Moore, et al. 2004. Early hematopoietic zinc finger protein (EHZF), the human homolog to mouse Evi3, is highly expressed in primitive human hematopoietic cells. *Blood*. 103:2062–2070. http://dx.doi.org/10.1182/blood-2003-07-2388

Chaki, M., R. Airik, A.K. Ghosh, R.H. Giles, R. Chen, G.G. Slaats, H. Wang, T.W. Hurd, W. Zhou, A. Cluckey, et al. 2012. Exome capture reveals ZNF423 and CEP164 mutations, linking renal ciliopathies to DNA damage response signaling. *Cell*. 150:533–548. http://dx.doi.org/10.1016/j.cell.2012.06.028

Cheng, L.E., and R.R. Reed. 2007. Zfp423/OAZ participates in a developmental switch during olfactory neurogenesis. *Neuron*. 54:547–557. http://dx.doi.org/10.1016/j.neuron.2007.04.029

Cheng, L.E., J. Zhang, and R.R. Reed. 2007. The transcription factor Zfp423/OAZ is required for cerebellar development and CNS midline patterning. *Dev. Biol*. 307:43–52. http://dx.doi.org/10.1016/j.ydbio.2007.04.005

Davidsson, J., H. Lilljebjörn, A. Andersson, S. Veerla, J. Heldrup, M. Behrendtz, T. Fioretos, and B. Johansson. 2009. The DNA methylome of pediatric acute lymphoblastic leukemia. *Hum. Mol. Genet*. 18:4054–4065. http://dx.doi.org/10.1093/hmg/ddp354

Ehrlich, M. 2002. DNA methylation in cancer: too much, but also too little. *Oncogene*. 21:5400–5413. http://dx.doi.org/10.1038/sj.onc.1205651

Escherich, G., M.A. Horstmann, M. Zimmermann, and G.E. Janka-Schaub; COALL study group. 2010. Cooperative study group for childhood acute lymphoblastic leukaemia (COALL): long-term results of trials 82,85,89,92 and 97. *Leukemia*. 24:298–308. http://dx.doi.org/10.1038/leu.2009.249

Feinberg, A.P., and B. Tycko. 2004. The history of cancer epigenetics. *Nat. Rev. Cancer*. 4:143–153. http://dx.doi.org/10.1038/nrc1279

Gronemeyer, H., and A. Zelent. 2009. Fingering modulators of retinoic acid signaling identifies new prognostic marker for neuroblastoma. *Cancer Cell*. 15:249–251. http://dx.doi.org/10.1016/j.ccr.2009.03.012

Hata, A., J. Seoane, G. Lagna, E. Montalvo, A. Hemmati-Brivanlou, and J. Massagué. 2000. OAZ uses distinct DNA- and protein-binding zinc fingers in separate BMP-Smad and Olf signaling pathways. *Cell*. 100:229–240. http://dx.doi.org/10.1016/S0092-8674(00)81561-5

Huang, S., J. Laoukili, M.T. Epping, J. Koster, M. Hölzel, B.A. Westerman, W. Nijkamp, A. Hata, S. Asgharzadeh, R.C. Seeger, et al. 2009. ZNF423 is critically required for retinoic acid-induced differentiation and is a marker of neuroblastoma outcome. *Cancer Cell*. 15:328–340. http://dx.doi.org/10.1016/j.ccr.2009.02.023

Kitamura, D., A. Kudo, S. Schaal, W. Müller, F. Melchers, and K. Rajewsky. 1992. A critical role of lambda 5 protein in B cell development. *Cell*. 69:823–831. http://dx.doi.org/10.1016/0092-8674(92)90293-L

Klug, M., and M. Rehli. 2006. Functional analysis of promoter CpG methylation using a CpG-free luciferase reporter vector. *Epigenetics*. 1:127–130. http://dx.doi.org/10.4161/epi.1.3.3327

Lauberth, S.M., and M. Rauchman. 2006. A conserved 12-amino acid motif in Sall1 recruits the nucleosome remodeling and deacetylase corepressor complex. *J. Biol. Chem*. 281:23922–23931. http://dx.doi.org/10.1074/jbc.M513461200

Lee, K.S., H.J. Kim, Q.L. Li, X.Z. Chi, C. Ueta, T. Komori, J.M. Wozney, E.G. Kim, J.Y. Choi, H.M. Ryoo, and S.C. Bae. 2000. Runx2 is a common target of transforming growth factor beta1 and bone morphogenetic protein 2, and cooperation between Runx2 and Smad5 induces osteoblast-specific gene expression in the pluripotent mesenchymal precursor cell line C2C12. *Mol. Cell. Biol*. 20:8783–8792. http://dx.doi.org/10.1128/MCB.20.23.8783-8792.2000

Lewin, J., A.O. Schmitt, P. Adorján, T. Hildmann, and C. Piepenbrock. 2004. Quantitative DNA methylation analysis based on four-dye trace data from direct sequencing of PCR amplificates. *Bioinformatics*. 20:3005–3012. http://dx.doi.org/10.1093/bioinformatics/bth346

Lin, A.C., A.E. Roche, J. Wilk, and E.C. Svensson. 2004. The N termini of Friend of GATA (FOG) proteins define a novel transcriptional repression motif and a superfamily of transcriptional repressors. *J. Biol. Chem*. 279:55017–55023. http://dx.doi.org/10.1074/jbc.M411240200

Miyazaki, K., N. Yamasaki, H. Oda, T. Kuwata, Y. Kanno, M. Miyazaki, Y. Komeno, J. Kitaura, Z. Honda, S. Warming, et al. 2009. Enhanced expression of p210BCR/ABL and aberrant expression of Zfp423/ZNF423 induce blast crisis of chronic myelogenous leukemia. *Blood*. 113:4702–4710. http://dx.doi.org/10.1182/blood-2007-05-088724

Mullighan, C.G., S. Goorha, I. Radtke, C.B. Miller, E. Coustan-Smith, J.D. Dalton, K. Girtman, S. Mathew, J. Ma, S.B. Pounds, et al. 2007. Genome-wide analysis of genetic alterations in acute lymphoblastic leukaemia. *Nature*. 446:758–764. http://dx.doi.org/10.1038/nature05690

Mullighan, C.G., X. Su, J. Zhang, I. Radtke, L.A. Phillips, C.B. Miller, J. Ma, W. Liu, C. Cheng, B.A. Schulman, et al; Children's Oncology Group. 2009. Deletion of IKZF1 and prognosis in acute lymphoblastic leukemia. *N. Engl. J. Med*. 360:470–480. http://dx.doi.org/10.1056/NEJMoa0808253

Mundt, C., S. Licence, T. Shimizu, F. Melchers, and I.L. Mårtensson. 2001. Loss of precursor B cell expansion but not allelic exclusion in VpreB1/VpreB2 double-deficient mice. *J. Exp. Med*. 193:435–445. http://dx.doi.org/10.1084/jem.193.4.435

Niebuhr, B., N. Kriebitzsch, M. Fischer, K. Behrens, T. Günther, M. Alawi, U. Bergholz, U. Müller, S. Roscher, M. Ziegler, et al. 2013. Runx1 is essential at two stages of early murine B-cell development. *Blood*. 122:413–423. http://dx.doi.org/10.1182/blood-2013-01-480244

Nutt, S.L., A.M. Morrison, P. Dörfler, A. Rolink, and M. Busslinger. 1998. Identification of BSAP (Pax-5) target genes in early B-cell development by loss- and gain-of-function experiments. *EMBO J*. 17:2319–2333. http://dx.doi.org/10.1093/emboj/17.8.2319

Pui, C.H., M.V. Relling, and J.R. Downing. 2004. Acute lymphoblastic leukemia. *N. Engl. J. Med*. 350:1535–1548. http://dx.doi.org/10.1056/NEJMra023001

Shultz, L.D., B.L. Lyons, L.M. Burzenski, B. Gott, X. Chen, S. Chaleff, M. Kotb, S.D. Gillies, M. King, J. Mangada, et al. 2005. Human lymphoid and myeloid cell development in NOD/LtSz-scid IL2R gamma null mice engrafted with mobilized human hemopoietic stem cells. *J. Immunol*. 174:6477–6489.

Tsai, R.Y., and R.R. Reed. 1997. Cloning and functional characterization of Roaz, a zinc finger protein that interacts with O/E-1 to regulate gene

expression: implications for olfactory neuronal development. *J. Neurosci.* 17:4159–4169.

Tsai, R.Y., and R.R. Reed. 1998. Identification of DNA recognition sequences and protein interaction domains of the multiple-Zn-finger protein Roaz. *Mol. Cell. Biol.* 18:6447–6456.

Vaissière, T., C. Sawan, and Z. Herceg. 2008. Epigenetic interplay between histone modifications and DNA methylation in gene silencing. *Mutat. Res.* 659:40–48. http://dx.doi.org/10.1016/j.mrrev.2008.02.004

Warming, S., T. Suzuki, T.P. Yamaguchi, N.A. Jenkins, and N.G. Copeland. 2004. Early B-cell factor-associated zinc-finger gene is a frequent target of retroviral integration in murine B-cell lymphomas. *Oncogene.* 23: 2727–2731. http://dx.doi.org/10.1038/sj.onc.1207452

Zelent, A., M. Greaves, and T. Enver. 2004. Role of the TEL-AML1 fusion gene in the molecular pathogenesis of childhood acute lymphoblastic leukaemia. *Oncogene.* 23:4275–4283. http://dx.doi.org/10.1038/sj.onc.1207672

Zhang, J., C.G. Mullighan, R.C. Harvey, G. Wu, X. Chen, M. Edmonson, K.H. Buetow, W.L. Carroll, I.M. Chen, M. Devidas, et al. 2011. Key pathways are frequently mutated in high-risk childhood acute lymphoblastic leukemia: a report from the Children's Oncology Group. *Blood.* 118:3080–3087. http://dx.doi.org/10.1182/blood-2011-03-341412